Excitation Wavelength- and Medium-Dependent Photoluminescence of Reduced Nanostructured TiO_2 Films

Luca Mascaretti,[*,†,‡] Valeria Russo,[†,¶] Giorgio Zoppellaro,[‡] Andrea Lucotti,[§] Carlo S. Casari,[†,¶] Štěpán Kment,[‡] Alberto Naldoni,[‡] and Andrea Li Bassi[*,†,¶]

†*Micro- and Nanostructured Materials Laboratory, Department of Energy, Politecnico di Milano, via Ponzio 34/3, 20133, Milano, Italy*

‡*Regional Centre of Advanced Technologies and Materials, Faculty of Science, Palacký University, Šlechtitelů 27, 783 71 Olomouc, Czech Republic*

¶*Center for Nanoscience and Technology – IIT@Polimi, via G. Pascoli 70/3, 20133, Milano, Italy*

§*Department of Chemistry, Materials and Chemical Engineering "Giulio Natta", Politecnico di Milano, piazza Leonardo da Vinci 32, 20133, Milano, Italy*

E-mail: luca.mascaretti@upol.cz; andrea.libassi@polimi.it

Phone: +420 585634487; +39 0223996316

Abstract

The performance of TiO_2 nanomaterials in solar energy conversion applications can be tuned by means of thermal treatments in reducing atmospheres, which introduce defects (such as oxygen vacancies), allowing, for instance, a better charge transport or a higher photocatalytic activity. The characterization of these defects and the understanding of their role are pivotal to carefully engineer the properties of TiO_2, and,

among various methods, they have been addressed by photoluminescence (PL) spectroscopy. A definitive framework to describe the PL properties of TiO_2, however, is still lacking. In this work, we report on the PL of nanostructured anatase TiO_2 thin films, annealed in different atmospheres (oxidizing and reducing), and consider the effects of different excitation energies and different surrounding media on their PL spectra.

A broad PL signal centered around 1.8–2.0 eV is found for all the films with UV excitation in air as well as in vacuum, while the same measurements in ethanol lead to a blueshift and to intensity changes in the spectra. On the other hand, measurements with different sub-bandgap excitations show PL peaking at 1.8 eV, with an intensity trend only dependent on the thermal treatment and not on the surrounding medium. The results of PL spectroscopy, together with electron paramagnetic resonance spectroscopy, suggest the critical role of oxygen vacancies and Ti^{3+} ions as radiative recombination centers. The complex relationship between thermal treatments and PL data in the explored conditions is discussed, suggesting the importance of such investigations for a deeper understanding on the relationship between defects in TiO_2 and photoactivity.

Keywords

TiO_2; photoluminescence; reducing thermal treatments; electron/hole traps

1 Introduction

Nanostructured forms of titanium dioxide (TiO_2) have been extensively investigated in solar energy conversion applications, such as in dye-sensitized[1,2] and perovskite[3,4] solar cells, in photocatalysis,[5,6] and in photoelectrochemical (PEC) water splitting.[4,7] The performance of TiO_2 in these applications is strongly influenced not only by the nanoscale morphology and crystallinity (anatase, rutile or mixtures between them are typically employed), but also by the defect chemistry of the material.[6,7] Even without intentional modifications, TiO_2 is often characterized by a slight sub-stoichiometry, mostly related to oxygen vacancies (V_O),[8] which

account for its n-type conductivity. Since the 1950s it has been shown that conductivity of TiO_2 can be increased by thermal treatments in hydrogen (H_2), attributed to an increase of V_O concentration.[9] In recent years, the controlled introduction of defects in TiO_2 by means of reducing thermal treatments has gained a renewed interest to increase the material photoactivity in water splitting experiments[10,11] after the work of Chen *et al.* in 2011,[12] concerning the so-called "black titania".

The characterization of defect states in the bandgap of a semiconductor can be addressed with photoluminescence (PL) spectroscopy, which is considered as a simple and versatile tool to probe discrete electronic states.[13] However, this task is quite complex for TiO_2, as evidenced by the wide and sometimes conflicting literature on the PL properties of nanocrystalline TiO_2 materials.[14] Generally, it has been shown that anatase and rutile exhibit distinct PL bands in the visible[15–23] and near-infrared (NIR)[17,19,21,23] regions of the electromagnetic spectrum, respectively, while brookite is by far less investigated.[24] McHale and co-workers, in particular, have developed an interpretative model for these emissions:[19,25–27] i) a weak and phase-independent emission at about 2.95 eV is attributed to recombinations between self-trapped excitons; ii) the main visible emission in anatase is composed of a green component ("type 1 PL" or "green PL"), at about 2.25 eV, due to recombinations between shallowly-trapped electrons and deeply-trapped holes, and a red component ("type 2 PL" or "red PL"), at about 2.0 eV, due to recombinations between valence band holes and deeply-trapped electrons; iii) the NIR emission in rutile is assigned to radiative recombinations between valence band holes and deeply-trapped electrons.

Other works have suggested the role of surface state-mediated recombinations,[15,20] donor-to-acceptor transitions,[21] and of band bending[22] on the visible PL of anatase. Recently, Pallotti *et al.*[23] have also investigated the PL mechanisms of TiO_2 nanocrystalline films, confirming the results obtained by McHale's group for the PL of anatase and giving a deeper explanation for the PL of rutile.

From the complex framework discussed above, it is possible to infer that some open

issues are still present in the current understanding of PL properties of TiO_2 nanomaterials: i) unambiguous results are difficult to obtain as PL properties vary according to the material porosity, morphology and defectivity;[14] ii) in the case of hydrogenated or reduced TiO_2, PL measurements have mostly been reported as characterization tools to gain insights on the material photoactivity[28–30] (sometimes with misinterpretations, as pointed out in ref.[31]) rather than for in-depth analyses;[27] iii) few-studies have compared above- to below-bandgap excitations with the aim of probing different trap/defect states in the bandgap.[15,20,23,32]

In this work we consider nanostructured anatase TiO_2 thin films, prepared by Pulsed Laser Deposition (PLD), exhibiting different activities in PEC water splitting experiments based on different degrees of defectivity induced by thermal treatments, as reported in previous works.[33,34] A deeper understanding on their defect states is here addressed by performing PL experiments and considering: i) the effect of post-deposition thermal treatments in both oxidizing and reducing atmospheres; ii) the effect of the excitation energy, both above the bandgap energy (UV) and below (blue, green and red excitations, the last one being not previously reported); iii) the effect of the surrounding medium (air, ethanol and vacuum), to probe alternative recombination pathways of the photogenerated charges. The present results show a more complex occurrence of the green PL and red PL mechanisms with respect to previous studies. Indeed, the "activation" of the former appears strongly influenced by the annealing treatment and the excitation energy, on the contrary of the latter. A tentative model to interpret these results is also proposed. This model relies on the information on defect states provided by electron paramagnetic resonance (EPR) spectroscopy, which suggests the presence of Ti^{3+} ions as electron traps and oxygen-based radicals as hole traps.

2 Experimental

Synthesis and characterization of TiO_2 films. TiO_2 nanostructured films were synthesized according to previous studies.[33,34] The films were grown at room temperature by

ablating a TiO_2 (99.9%) target with a ns-pulsed laser (Nd:YAG, 2nd harmonic, $\lambda = 532$ nm, repetition rate 10 Hz, pulse duration 7 ns) at a background gas pressure of 5 Pa in an Ar/O_2 (50%-50%) atmosphere. The laser fluence on the target was set at about 3.5 J/cm^2 and the laser pulse energy was 170 mJ. Si (100) with 0.5 mm thickness (University Wafer) was employed as substrate material, since it has no PL contribution in the investigated region,[35] with a fixed target-to-substrate distance of 50 mm.

Two kinds of post-deposition annealing treatments were performed: a reference air annealing in a Lenton muffle furnace (4 °C min^{-1} heating ramp, 2 h dwell at 500 °C), and three double thermal treatments in reducing environments: i) air annealing followed by a thermal treatment in an Ar/H_2 (97%-3%) mixture at atmospheric pressure in a home-made furnace (10 °C min^{-1} heating ramp, 3 h dwell at 500 °C); ii) the same, but with the second step in Ar/H_2 substituted with a thermal treatment with the same temperature program in vacuum ($P < 3 \cdot 10^{-4}$ Pa); iii) air annealing followed by a thermal treatment in pure H_2. The samples are hereinafter labeled as follows: TiO_2 is the reference air-annealed film; TiO_2-AH is the film annealed in air and in Ar/H_2 mixture; TiO_2-V is the film annealed in air and in vacuum; TiO_2-H is the film annealed in air and in pure H_2 (as summarized in Table S1).

The morphological and structural analyses of these films were performed by scanning electron microscopy (SEM), Raman spectroscopy and X-ray diffraction (see Supporting Information). X-ray photoelectron spectroscopy (XPS) was performed at room temperature with monochromatized Al-Kα source. Electron paramagnetic resonance (EPR) spectroscopy was performed at $T = 143$ K in two different conditions: first, at the solid state in the dark; second, in water/methanol (H_2O/MeOH) solution (50/50, vol/vol) with 5 mg/mL phenyl-*N*-*ter*-butylnitrone (PBN) as spin trapping agent upon UV laser light irradiation (325 nm, 100 mW) for 5 min at 253 K. The simulation of the EPR traces was performed with the WinEPR SimFonia software (V.1.25) using second-order perturbation theory. Theoretical modeling of the spin-trapped radical adduct with estimation of the spin density distribution was obtained by density functional theory (DFT) using an unrestricted B3LYP functional.

Further details on the characterization of TiO_2 films, DFT simulations, and PL data fitting and normalization procedures are reported in Supporting Information.

Photoluminescence (PL) spectroscopy. Room temperature PL spectra were acquired at different excitation wavelengths employing Raman spectrometers; the following excitation wavelengths were chosen: UV at $\lambda = 325$ nm or $E_{exc} = 3.82$ eV (0.6 mW power), blue at $\lambda = 457$ nm or $E_{exc} = 2.71$ eV (1 mW power), green at $\lambda = 514.5$ nm or $E_{exc} = 2.41$ eV (1 mW power), and red at $\lambda = 633$ nm or $E_{exc} = 1.96$ eV (3 mW power). Measurements in ethanol (95% purity) were performed in a quartz cuvette, while in vacuum by placing the sample into a cryostat connected to a diaphragm pump (see Supporting Information for additional details).

3 Results and discussion

3.1 XPS and EPR characterization

Crystalline anatase TiO_2 films were characterized by a vertically-oriented mesostructure with nanoscale porosity resulting from the assembling of fine nanoparticles of about 10 nm in size (Figure S1), confirming previous investigations employing similar synthesis conditions.[33,34,36–38] The films exhibit interference colors due to their low thickness (about 280 nm) and the high reflectance of the Si substrate. As a consequence, their reflectance (not shown) did not exhibit major differences related to the annealing process (see the optical analysis in previous works on thicker films deposited on glass substrates).[33,34]

The electronic properties of TiO_2 films were investigated by valence band XPS, as reported in Figure 1. For the TiO_2 (annealed in air) and TiO_2-H (annealed in air and in pure H_2) films, the band edge was found at 2.66 and 2.63 eV (with the Fermi level $E_F = 0$ in Figure 1), respectively, while slightly lower values were found for the TiO_2-AH (annealed in air and in Ar/H_2 mixture) and TiO_2-V (annealed in air and in vacuum) films (2.54 and 2.52 eV, respectively).

On average, considering an experimental error of $\simeq$ 0.1 eV, we determined an offset between the conduction band edge (E_c) and E_F of 0.6 eV, consistent with other reports.[39,40] This value suggests the n-type conductivity of TiO_2 with a relatively low doping level, which may be ascribed to the effect of the first annealing step in air. A low doping level is also consistent with optical measurements reported in our previous studies[33,34] and with EPR measurements at the solid state (Figure 2, see below). In addition, no substantial VB shift was found upon reduction/hydrogenation (i.e. $\simeq$ 0.1 eV), similarly to previous reports[39–41] and contrarily to others.[12,42] The density of states (DOS) in the VB exhibited two main features, i.e. one at $\sim$ 7 eV, mainly constituted by Ti 3d orbitals, and one at $\sim$ 5 eV, mainly made up of O 2p orbitals.[43–45] The intensity of the latter was slightly lower in TiO_2-AH and in TiO_2-V films, which may suggest a higher sub-stoichiometry for these films. However, no peak at 1.0 eV below E_F was found, which has been attributed to the presence of Ti^{3+} on the surface.[43,46] Indeed, the Ti 2p and O 1s XPS spectra did not evidence any clear change between the TiO_2 film and all the other ones treated in reducing conditions (Figure S2 and Table S2). This finding can be attributed to the effect of air exposure (which could not be prevented during samples handling), i.e. most of the V_O present at the surface would be "healed" by O_2 molecules in air. As a consequence, the overall XPS analysis suggested that the surface of all the annealed TiO_2 films was substantially stoichiometric, i.e. the concentration of defects in the surface layers of the films was lower than the detection limit of XPS.

EPR spectroscopy was employed to probe the presence of spin-containing defects in the TiO_2 films. All the samples showed the presence of weak resonances (Figure 2), which, based on their shape and position, can be assigned to the formation of Ti^{3+} sites ($3d^1$, $S = 1/2$) in regular lattice positions in distorted tetragonal fields (with $g_\perp > g_\parallel$).[47,48] The distortion was associated with a variation of Ti–O bond lengths due to the different charge (Ti^{3+} vs. Ti^{4+}) and with the change of effective spin ($3d^1$ vs $3d^0$). Representative spectra of the materials are shown in Figure 2a for the TiO_2 film, 2b for the TiO_2-AH film, and 2c for the

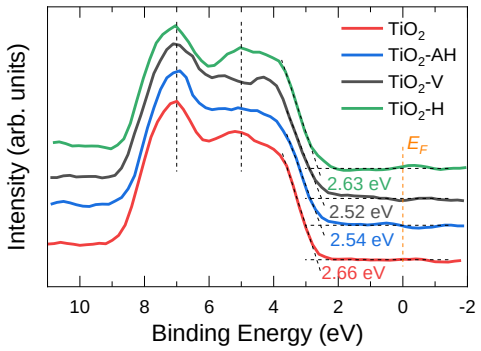

Figure 1: Valence band XPS spectra of annealed TiO_2 films. Black dashed lines highlight the features at $\sim$ 7 and $\sim$ 5 eV mainly constituted by Ti 3d and O 2p orbitals, respectively. An orange dashed line highlights the Fermi level at 0 eV.

TiO_2-V film, while the simulated EPR trace (*via* perturbation theory) of lattice-embedded Ti^{3+} cations in the anatase phase is given in Figure 2d. A quantitative comparison of the spin concentration in these materials was not possible, due to experimental difficulties on loading identical amount of thin films into the tubes and due to the very low concentration of paramagnetic Ti^{3+} species detected.

Ti^{3+} states can be formed by the release of electrons from a doubly-ionized oxygen vacancy (which becomes neutral),[8]

$$O^{2-} + 2\,Ti^{4+} \rightleftharpoons {V_O}^{2-} + 2\,Ti^{4+} + \frac{1}{2}O_2(g) \rightleftharpoons V_O + 2\,Ti^{3+} + \frac{1}{2}O_2(g) \tag{1}$$

where it is assumed for simplicity that all the species are located at regular lattice sites.[49] On the other hand, such states can be originated also in stoichiometric TiO_2 upon photogeneration (Equation (2)) by electron trapping (Equation (3)); electrons can be also trapped by oxygen vacancies (Equation (4)):

$$TiO_2 + h\nu \longrightarrow {e_{CB}}^- + {h_{VB}}^+ \tag{2}$$

$$Ti^{4+} + {e_{CB}}^- \rightleftharpoons Ti^{3+} \tag{3}$$

$${V_O}^- + {e_{CB}}^- \rightleftharpoons {V_O}^{2-} \tag{4}$$

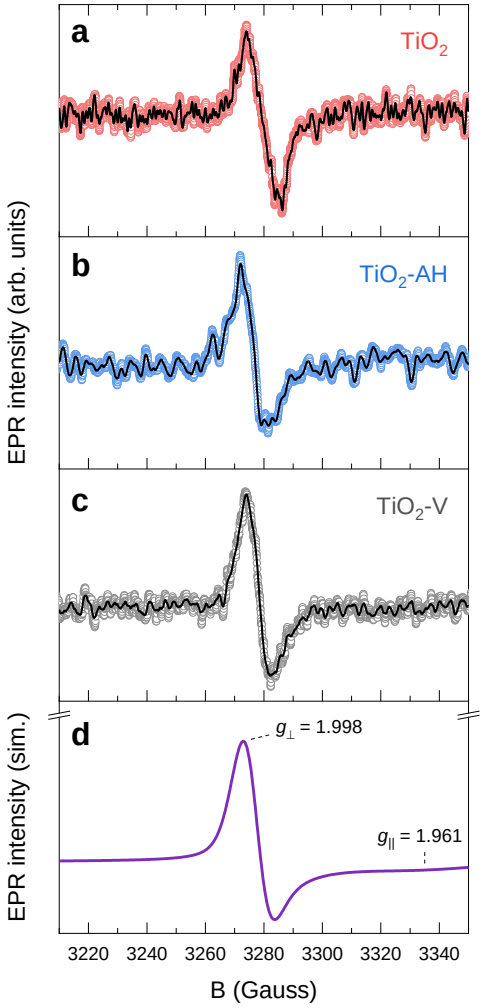

Figure 2: Experimental X-band EPR spectra (9.15 GHz) of **a)** TiO_2, **b)** TiO_2-AH and **c)** TiO_2-V films recorded at $T = 143$ K. Experimental parameters: microwave power 3.8 mW (b), 2.8 mW (b and c). **d)** Simulated Ti^{3+} resonance signal (frequency 9.15 GHz) as obtained from second-order perturbation theory, with spin-Hamiltonian parameters $g_{x,y} = 1.998$, $g_z = 1.961$, Lorentzian/Gaussian ratio of 0.63, line-width tensor ($L_{x,y,z}$) of 8.0,7.0,40.0 Gauss. The bold lines in (a–c) correspond to the resolution-enhanced EPR resonance signals (Savitzky-Golay, denoise algorithm).

Irrespectively of the precise mechanism, EPR measurements in Figure 2 suggested the presence at equilibrium (without prior light illumination) of Ti^{3+} sites in regular lattice positions, thus not exposed at the surface. The absence of major differences in the spectra among the films with different annealing treatments and the lack of specific Ti^{3+} features in XPS measurements (Figures 1 and S2) is consistent with slightly reduced titanium dioxide materials, i.e. TiO_{2-x}.

To achieve a better understanding on the defect-mediated charge transfer properties at the surface of TiO_2 materials, relevant in terms of photocatalytic applications, we employed EPR spectroscopy in conjunction with spin-trapping experiments, using phenyl-*N*-*ter*-butylnitrone (PBN) as the chemical trapping agent. The experimental strategy is schematically illustrated in Figure 3a. The TiO_2 materials were placed inside the EPR tubes in H_2O/MeOH solution containing PBN. The solutions were irradiated inside the EPR cavity with an UV laser source (325 nm), allowing the photogeneration of electron-hole pairs in TiO_2 (Equation (2)). Thus, photogenerated holes could react with MeOH leading to the methoxy radical ($CH_3O^\bullet$)[50] and this radical could be trapped by PBN, leading to the EPR-active species PBN–$CH_3O^\bullet$ (Figures S3 and S4). After few minutes, necessary to cool down the tubes at $T = 143$ K, EPR spectra were acquired, showing a clear signature of the trapped PBN–$CH_3O^\bullet$ radicals, as highlighted by the blue segment in Figures 3b and 3c for the TiO_2 and TiO_2-H films, respectively (the TiO_2-AH and TiO_2-V films showed similar spectra to the TiO_2-H film and are thus not reported). However, it has been reported that TiO_2 under UV irradiation may decompose methanol to the OH–$CH_2^\bullet$ species,[51] which would lead to the EPR active species PBN–$CH_2OH^\bullet$. As a consequence, the close resemblance of the simulation of the EPR resonance of the PBN–$CH_3O^\bullet$ species in Figure 3d to the experimental traces in Figures 3b and 3c confirmed the formation of the methoxy radical in our experimental conditions. The formation of this species suggests that all the TiO_2 materials are active catalysts for the water splitting process in the presence of methanol as sacrificial agent (see also the Discussion section).

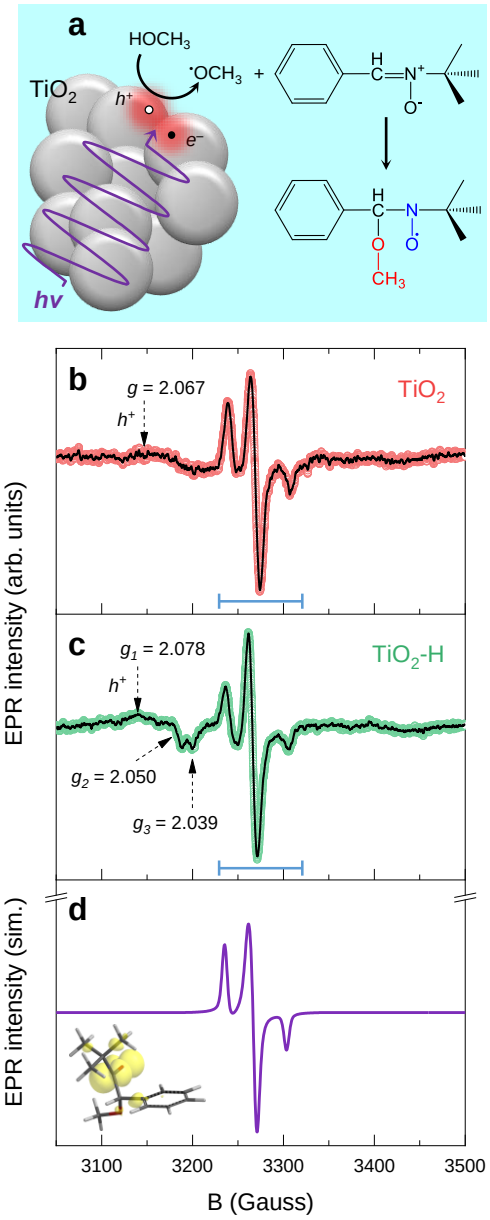

Figure 3: a) Schematic of the EPR measurements in H_2O/MeOH in the presence of PBN as spin-trapping agent after UV irradiation and experimental spectra of **b)** TiO_2 and **c)** TiO_2-H films (experimental parameters: frequency 9.140 GHz (b), 9.134 GHz (c), applied power 3.6 mW (b) and 2.8 mW (c), time constant 0.03 s, modulation width 6 Gauss and $T = 143$ K). **d)** Simulated EPR trace (frequency 9.134 GHz) of the PBN–$CH_3O^{\bullet}$ (neutral) radical and its optimized structure by DFT (UB3LYP/6-31G*, $E = -673.232495$ au) with the spin density isosurface drawn at IsoVal of 0.002 au. The following spin-Hamiltonian parameters were obtained: $g_{xx} = 2.0069$, $g_{yy} = 2.0048$, $g_{zz} = 2.0022$, $A_{zz}(^{14}N) = 33.5$ Gauss, $A_{yy}(^{14}N) = 4.0$ Gauss, Lorentzian/Gaussian ratio= 0.6 (spherical integration using θ,ϕ of 200,200).

On the other hand, not all the photogenerated holes reacted with methanol, giving the methoxy radical and, thus, PBN–$CH_3O^{\bullet}$. Indeed, additional resonances appeared in the EPR spectra in Figures 3b and 3c, attributed to the formation of trapped holes ($h_{trap}{}^{+}$, oxygen-based radicals, i.e. Ti^{4+}–$O^{\bullet}$),[52] with g-values given in the EPR plots (see also the simulated EPR signal in Figure S5). In particular, the broad EPR signals with resonances at $g = 2.067$ and $g_1 = 2.078$ for the TiO_2 (Figure 3a) and TiO_2-H (Figure 3b) films, respectively, could be associated to holes trapped at the surface of TiO_2. Additionally, the sample TiO_2-H showed two other signals at $g_2 = 2.050$ and $g_3 = 2.039$, which could be related to a different type (e.g. sub-layer) of trapped holes experiencing lower g-anisotropy, possibly related to the second annealing step in H_2. In the bulk, indeed, holes are trapped by lattice oxygen sites upon photoexcitation (Equation (2)):[8]

$$O^{2-} + h_{VB}{}^{+} \rightleftharpoons O^{-} \tag{5}$$

Other hole trapping sites suggested in the literature are bridging $O^{\bullet-}$ or $OH^{\bullet}$ surface sites[6] and surface OH groups bound to low-coordinated Ti atoms at the surface of nanoparticles.[53] A clear assignment of the features in Figure 3 to a specific chemical species was not possible; however, our observations suggest that i) both oxidized and reduced TiO_2 thin films exhibit the presence of trapped holes even in the presence of methanol (which acts as a hole scavenger),[54] and ii) the reducing thermal treatment introduces additional trapped hole states (the g_2 and g_3 features in Figures 3c and S5). Thus, EPR measurements with the spin trapping technique gave information on hole traps, detected upon UV light irradiation, adding information to EPR experiments in the dark, which gave information on electron traps (Figure 2). These species of traps can be active recombination centers for photogenerated charges, giving rise to different PL mechanisms in anatase TiO_2, as discussed in the following.

3.2 PL measurements in air

The PL spectra of the TiO_2 films, measured in air with all the investigated excitation wavelengths, are shown in Figure 4. PL spectra with UV excitation (3.82 eV, Figure 4a) showed a similar spectral shape for all the films, with the highest intensity detected for the TiO_2-AH film. The PL maximum was found approximately at 2.0 eV, with a large Stokes shift with respect to the excitation energy. Also with blue excitation (2.71 eV, Figure 4b) the maximum PL intensity was shown by the TiO_2-AH film at about 2.1 eV; this was slightly shifted with respect to the maximum exhibited by the TiO_2-H and TiO_2-V films (at about 2.2 eV). Moreover, the TiO_2 film did not show any signal at all. A somehow similar outcome was found with green excitation (2.41 eV, Figure 4c): also in this case the TiO_2 film had no emission. The TiO_2-AH film clearly showed the highest intensity, followed by the TiO_2-H and TiO_2-V films (close to each other). The PL curve maxima were found at about 1.8–1.9 eV. Finally, with red excitation (1.96 eV, Figure 4d) the intensity trend was the same as with the other excitation energies and the TiO_2 film did not show any PL emission (the signal at energy below 1.3 eV is due to the PL of Si substrate).[35]

The thickness (about 280 nm) of the films considered in this study prevents any interference effect, being lower than the lowest excitation wavelength (UV, 325 nm);[55,56] for this reason, PL spectra were fitted with a superposition of Gaussian curves (see Figures S6–S9 and Tables S3–S6 for the details). The fit results are summarized in Table 1. Each individual Gaussian component was labeled as $PL_{n,\lambda}$, where $n = 1, 2, 3...$ and λ is the excitation wavelength (UV, blue, green or red), having energy $\varepsilon_{n,\lambda}$ (eV). In addition, when at least two components emerged from a fit procedure, the ratio between the area under the n-th component and the first one, defined as $\alpha_{n,\lambda} = A(PL_{n,\lambda})/A(PL_{1,\lambda})$ was calculated (Tables S3–S6) and reported in Table 1 accordingly (in brackets).

With UV excitation (Figure 4a), the experimental PL curves of all the annealed films could be fitted with three Gaussian components, peaked in the red ($\varepsilon_{1,\mathrm{UV}} = 1.80$ eV), orange ($\varepsilon_{2,\mathrm{UV}} = 1.97$ eV), and yellow ($\varepsilon_{3,\mathrm{UV}} = 2.17$ eV) regions of the visible electromagnetic

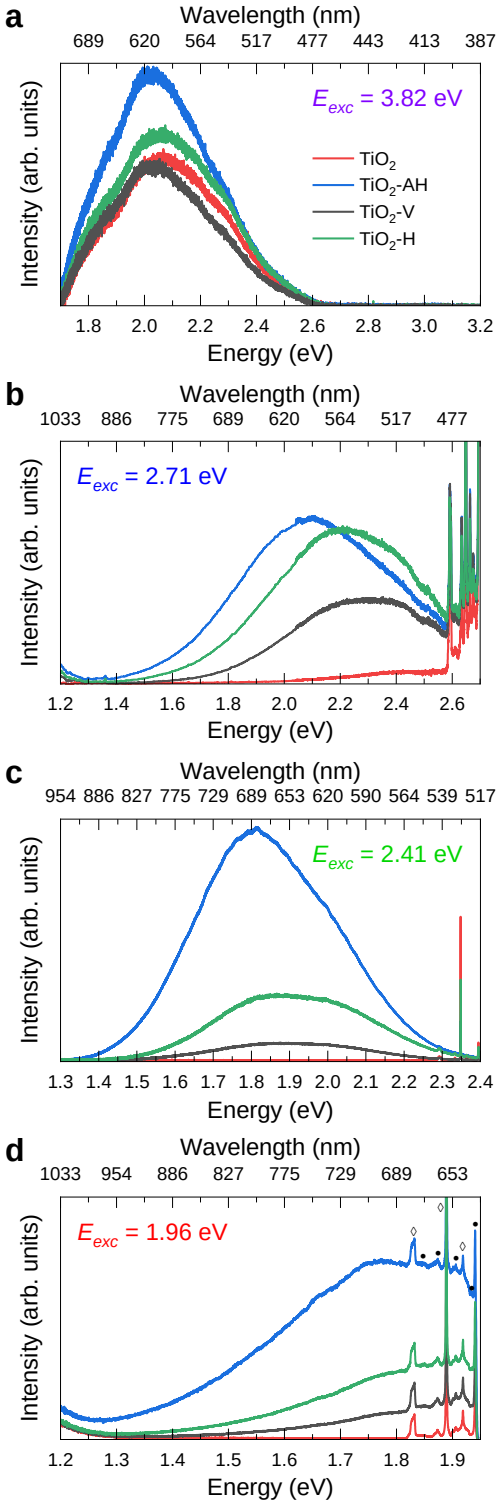

Figure 4: Photoluminescence spectra of annealed films (red: TiO_2; blue: TiO_2-AH; black: TiO_2-V; green: TiO_2-H) with different excitation energies: **a)** 3.82 eV (UV), **b)** 2.71 eV (blue), **c)** 2.41 eV (green), **d)** 1.96 eV (red). Raman peaks, corresponding to the anatase phase (•) and Si substrate (◇), appear on the right part of spectra in b–d (see Figure S1b) due to the vicinity between the excitation energy and the PL emission (the spectral assignment is reported only in d for clarity).

spectrum, with very similar values of $\alpha_{n,\lambda}$ (see Table 1). With blue excitation (Figure 4b), a good fit of the experimental curves was achieved employing a single Gaussian peak for the TiO_2-V and TiO_2-H films (with $\varepsilon_{1,\text{blue}} = 2.30$ and 2.23 eV, respectively, both in the green visible region), while two peaks were needed for the TiO_2-AH film (with $\varepsilon_{1,\text{blue}} = 2.10$ eV and $\varepsilon_{2,\text{blue}} = 2.52$ eV, in the yellow and blue-green visible regions, with the first component clearly more intense and wider than the second one). With green excitation (Figure 4c), in all cases two Gaussian components were found, peaked in the red ($\varepsilon_{1,\text{green}} = 1.79$–$1.85$ eV) and orange ($\varepsilon_{2,\text{green}} = 2.03$–$2.06$ eV) regions of the visible spectrum. In particular, the $PL_{1,\text{green}}$ component is larger than the $PL_{2,\text{green}}$ one, but for the TiO_2-H film they have similar intensity ($\alpha_{2,\text{green}} = 0.99$). With red excitation (Figure 4d), finally, the PL spectra of all the double-treated films could be fitted by forcing a single Gaussian peak in the interval 1.79–1.87 eV, i.e. in the visible region at red wavelengths.

Table 1: Peak position values obtained from the multi-Gaussian fit of PL spectra presented in Figure 4. The numbers in brackets represent the $\alpha_{n,\lambda}$ values ($\alpha_{n,\lambda} = A(PL_{n,\lambda})/A(PL_{1,\lambda})$). The error estimate is $e = 0.05$ eV.

Exc.	Peaks	TiO_2	TiO_2-AH	TiO_2-V	TiO_2-H
UV	$PL_{1,UV}$	1.81 eV	1.80 eV	1.81 eV	1.81 eV
	$PL_{2,UV}$	1.98 eV *(5.20)*	1.98 eV *(5.83)*	1.98 eV *(5.45)*	1.97 eV *(4.68)*
	$PL_{3,UV}$	2.18 eV *(10.69)*	2.17 eV *(8.53)*	2.17 eV *(8.04)*	2.18 eV *(9.79)*
Blue	$PL_{1,\text{blue}}$	-	2.10 eV	2.30 eV	2.23 eV
	$PL_{2,\text{blue}}$	-	2.52 eV *(0.09)*	-	-
Green	$PL_{1,\text{green}}$	-	1.79 eV	1.85 eV	1.80 eV
	$PL_{2,\text{green}}$	-	2.05 eV *(0.27)*	2.06 eV *(0.38)*	2.03 eV *(0.99)*
Red	$PL_{1,\text{red}}$	-	1.81 eV	1.85 eV	1.87 eV

By overall considering the experimental data in Figure 4 and the fitting analysis in Table 1, some observations can be pointed out: i) for UV excitation, comparable results for all the investigated films were found, independently on the specific thermal treatment; ii) the films treated with a second step in reducing atmosphere exhibit PL emissions with below-bandgap excitation, on the contrary of the TiO_2 film; iii) the TiO_2-AH films showed the highest PL intensity for all the excitation wavelengths; iv) in general, all the PL bands

are centered around 1.8–2.2 eV and they exhibit some components with very similar energies for different films and for different excitation energies: $\varepsilon_{1,\mathrm{UV}} = \varepsilon_{1,\mathrm{green}} = \varepsilon_{1,\mathrm{red}}$ and $\varepsilon_{2,\mathrm{UV}} \simeq \varepsilon_{2,\mathrm{green}}$. The last point may suggest that the observed PL mechanism was the same and that the different excitation energies allowed to probe various components of the overall emission: for instance, with UV excitation the "complete" PL emission could be investigated.

3.3 Effect of the surrounding environment

With the aim of evaluating the charge transfer properties of the TiO_2 films with the surrounding environment, PL measurements were performed in liquid ethanol and in vacuum, and compared to the results obtained in air. Indeed, O_2 molecules in air can scavenge photogenerated electrons in the conduction band of TiO_2 or trapped electrons, which does not occurr in vacuum; ethanol, conversely, can scavenge valence band holes.[54,57] Moreover, the same hole scavenging effect is common among several alcohols, including methanol, thus the PL results in ethanol (see below) can be related to the EPR results with the spin trapping agent (Figure 3). To this purpose, two excitation wavelengths were selected, one above the bandgap energy (UV) and one below (green); accordingly, the results are presented in Figure 5.

Measurements with UV excitation (Figures 5a and 5b) revealed a change in the intensity trend with respect to the measurements in air (Figure 4). In particular, in the case of ethanol (Figure 5a), the TiO_2-H film showed the highest intensity, followed by the TiO_2-AH, TiO_2-V, and TiO_2 films. Notably, the latter exhibited a very weak and broad spectrum. Moreover, for all these films, a change in the spectral shape and a blueshift emerged with respect to measurements in air. On the other hand, the PL curves recorded in vacuum (Figure 5b) showed a spectral trend comparable to that measured in air (i.e. without any substantial shift/broadening, see Figure 4a), but, surprisingly, the intensities were almost the same for all the films.

With green excitation, both in ethanol and in vacuum (Figures 5c and 5d, respectively),

similar PL curves as those measured in air (Figure 4c) were obtained; indeed, the spectra did not exhibit any shift or broadening, and the intensity trend with respect to the annealing treatment did not change, i.e. TiO_2-AH > TiO_2-H > TiO_2-V > $TiO_2 \simeq 0$. The only relevant difference is the appearance of ethanol Raman peaks in Figure 5c due to their superposition with the TiO_2 PL curve excited at 2.41 eV; this feature did not substantially affect the PL curves.

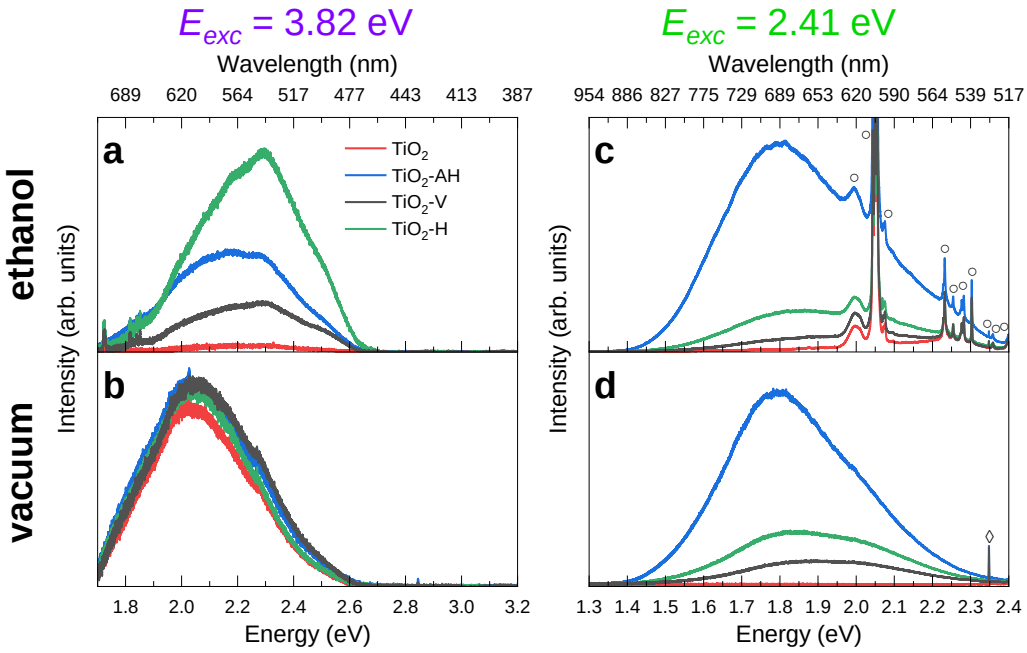

Figure 5: Photoluminescence spectra of annealed films (red: TiO_2; blue: TiO_2-AH; black: TiO_2-V; green: TiO_2-H) with UV **(a, b)** and green **(c, d)** excitations in ethanol **(a, c)** and in vacuum **(b, d)**. Raman peaks, corresponding to ethanol (○) and Si substrate (◇), appear on the right part of spectra in c and d due to the vicinity between the excitation energy and the PL emission.

To gain further understanding on the PL curves obtained with UV excitation, Figure 6 illustrates the effect of the surrounding atmosphere for each of the annealed TiO_2 films; in each case, the curve obtained in air was taken as reference and a normalization procedure was employed to qualitatively compare the intensities measured in the different experimental conditions (see Supporting Information). For the TiO_2 film (Figure 6a), an evident intensity decrease and broadening occurred for the PL measurement in ethanol with respect to that in air; in vacuum, conversely, the intensity increased without any substantial spectral shift. For the TiO_2-AH and TiO_2-V films (Figure 6b and 6c, respectively), conversely, the measurement

in ethanol led to a slight intensity decrease and to a blueshift compared to the emission recorded in air. The measurement in vacuum, on the other hand, led to equal and higher intensity to the measurement in air for the TiO_2-AH and TiO_2-V films, respectively. Finally, for the TiO_2-H film (Figure 6d), the PL curve recorded in vacuum showed a slightly higher intensity than that measured in air, while a clearly higher intensity and a substantial blueshift was observed with the measurement in ethanol.

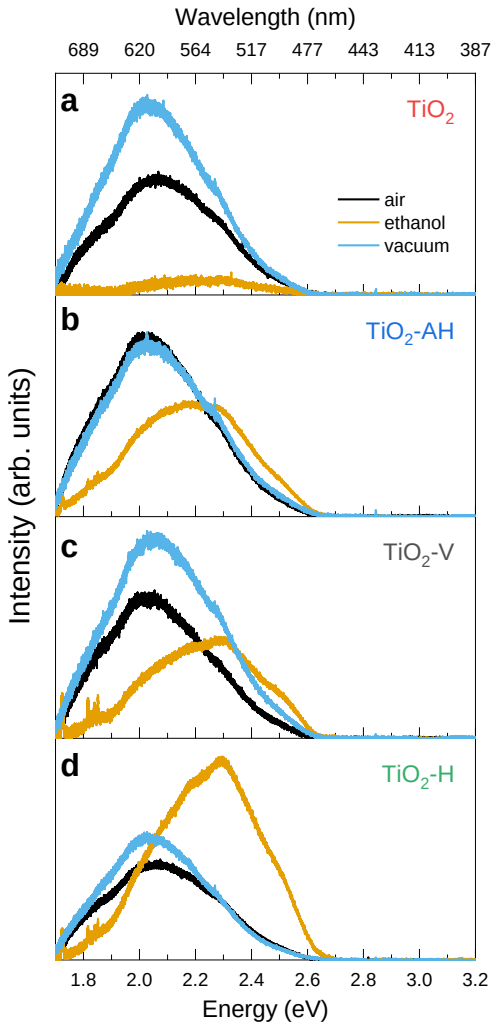

Figure 6: Effect of the surrounding environment on the PL emission of annealed TiO_2 films with UV excitation. **a)** TiO_2; **b)** TiO_2-AH; **c)** TiO_2-V; **d)** TiO_2-H.

As for the measurements in air, the multi-Gaussian fitting of the PL curves measured in ethanol and in vacuum is reported in Figures S6–S9 and Tables S3–S6. Table 2 summarizes

only the results obtained in ethanol with UV excitation, as only in these conditions an evident spectral change with respect to the measurements in air was observed. For the TiO_2 film, only one broad Gaussian peak with $\varepsilon_{1,UV} = 2.22$ eV was found (i.e. in green visible region), which was considered unreliable due to the very low signal/noise ratio of the PL curve (see Figure S6b). Conversely, for all the films treated in reducing atmospheres, five Gaussian components were found; interestingly, the first three ones ($PL_{1,UV}$, $PL_{2,UV}$, and $PL_{3,UV}$) exhibited a very similar energy to the corresponding components with air as surrounding medium, i.e. at red, orange and yellow wavelengths of the visible electromagnetic spectrum. The two additional components, i.e. $PL_{4,UV}$ and $PL_{5,UV}$, appeared at 2.30–2.33 eV (green) and 2.49–2.51 eV (blue-green), respectively. Furthermore, the relative intensities between these components varied from film to film: the most intense one was the yellow component ($\alpha_{3,UV} = 7.56$) for the TiO_2-AH film and the green component for the TiO_2-V and TiO_2-H films ($\alpha_{4,UV} = 5.41$ and $\alpha_{4,UV} = 5.42$, respectively).

Table 2: Peak position values obtained from the multi-Gaussian fit of PL spectra recorded with UV excitation in ethanol Figure 5. The numbers in brackets represent the $\alpha_{n,\lambda}$ values (see the text for the definition). The error estimate is $e = 0.05$ eV. *This value is considered not reliable.

Exc.	Peaks	TiO_2	TiO_2-AH	TiO_2-V	TiO_2-H
UV	$PL_{1,UV}$	2.22 eV*	1.84 eV	1.88 eV	1.93 eV
	$PL_{2,UV}$	-	1.98 eV *(0.40)*	1.99 eV *(0.40)*	2.01 eV *(0.62)*
	$PL_{3,UV}$	-	2.13 eV *(7.56)*	2.10 eV *(2.54)*	2.13 eV *(2.25)*
	$PL_{4,UV}$	-	2.33 eV *(2.77)*	2.30 eV *(5.41)*	2.31 eV *(5.42)*
	$PL_{5,UV}$	-	2.49 eV *(1.09)*	2.51 eV *(0.78)*	2.50 eV *(1.14)*

3.4 Discussion

With the aim of rationalizing the large set of PL results in relation to the electronic characterization and previous literature studies, a tentative scheme for the PL processes in the TiO_2 films is presented in Figure 7. This scheme adopts the same nomenclature for the red PL and green PL mechanisms to that reported by McHale and co-workers[19] and Pallotti *et al.*,[23] although a different assignment for the green PL-active states is proposed (see be-

low). In contrast to other literature reports, it does not support interpretation involving self-trapped exciton recombinations,[58] nor the effects of band bending,[22] the latter hardly occurring in a particle-assembled film.[59] In addition, we consider the time scales for charge generation, trapping and recombination processes based on previous literature studies.

Upon UV excitation, hot electron/hole pairs (i.e. excitons) are generated in the range of fs and migrate in shallow traps in 100-200 fs.[6] Shallow traps for electrons can participate in charge transport through a hopping mechanism, enhancing the conductivity of TiO_2,[60] and they have been represented with a width of 0.2 eV (grey-shaded area) below the conduction band minimum (E_c) based on the reported Urbach energy of anatase.[61] Accordingly, transmittance and reflectance measurements in previous works showed an absorption tail in the visible range in films prepared in analogous conditions, without major differences related to the thermal treatments.[33,34] Conversely, shallowly-trapped holes have not been discerned from valence band holes as previous studies suggest that they are in equilibrium (i.e. they have very similar energies).[62] The deep trapping for holes occurs in 200 fs, considerably faster than that for electrons (50–500 ps).[6,63] The widths of deep traps of electrons (1.0 eV) and holes (0.8 eV) have been represented based on the experimental width of the PL peaks. The position of these traps has been chosen according to the description of the red PL and green PL mechanisms given by McHale and co-workers.[19]

Notably, electron traps are represented below the Fermi level, which is located at 2.6 eV with respect to the valence band maximum (E_v) based on valence band XPS measurements (Figure 1). This can be considered as a lower limit of the $E_F - E_v$ offset, since E_F would be much closer to E_c (i.e. $\simeq 0.05$ eV instead of $\simeq 0.5$ eV) in strongly n-doped TiO_2 materials.[64] Nevertheless, this positioning of E_F allows the (partial) occupation of deep electron traps at equilibrium, in agreement with EPR results at the solid state (see below). On the other hand, the population of hole traps in Figure 7 occurs only upon photoexcitation, as suggested by EPR results with spin trapping (Figure 3). The recombination between trapped charges occurs in timescales of 20–200 ns.[6,62] Figure 7 also reports the surface reactions involving

the trapped charges, which compete with the recombination processes. On the one hand, O_2 molecules can scavenge either photogenerated electrons in the conduction band of TiO_2 or trapped electrons, thus forming the superoxide species, $O_2^{\bullet-}(ads)$, which occurs in 10–100 µs and 100 ns, respectively, while ethanol can scavenge valence band holes in 1 ns.[54,57] Figure 7 also reports a chemical assignment of electron and hole traps, based on previous literature studies and on the EPR results (Figures 2 and 3). Theoretical calculations suggested that shallow electron traps could be assigned to neutral oxygen vacancies (V_O^{2-}), while deep states to singly/doubly ionized vacancies (V_O^{-}/V_O).[65–67] Experiments have generally shown that deep defect levels around 0.75–1.00 eV from the anatase conduction band minimum could be related to oxygen vacancies and Ti^{3+} ions.[42,68,69] Accordingly, Figure 7 reports the labels V_O^{2-} and $V_O^{-}/V_O/Ti^{3+}$ for shallow and deep electron traps, respectively. Ti^{3+} ions not exposed to the surface (as suggested by EPR) would be less sensitive to the scavenging effects of O_2 molecules as well as their vacancy-healing effect.[69] Thus, as they would lie below the Fermi energy, they could be populated by electrons at equilibrium, also if TiO_2 were in contact with molecular O_2. Conversely, deep hole traps have been associated to surface or sub-surface oxygen-based radicals ($O^{\bullet}$) based on EPR results with spin trapping (Figure 3) and literature studies.[6,8,53] This assignment is different from the one developed by McHale and co-workers[19] and Pallotti *et al.*,[23] who related such traps to oxygen vacancies. Apart from their unequivocal identification, which was not possible in this work, the location of hole traps on the surface is in agreement with previous literature.[6,19,23,53]

PL with UV excitation. The PL curves reported in Figure 4a, i.e. with UV excitation in air, could be interpreted in terms of the red PL mechanism reported by McHale and co-workers[19,25–27] and Pallotti *et al.*,[23] i.e. radiative recombinations between electrons in deep traps and valence band holes. The absence of the green PL mechanism, i.e. radiative recombinations between free or shallowly-trapped electrons and deeply-trapped holes, could be ascribed to the quenching effect of O_2 molecules. Electrons in deep traps (on the energy scale), conversely, would not be scavenged by O_2, leading to a stronger red PL with UV

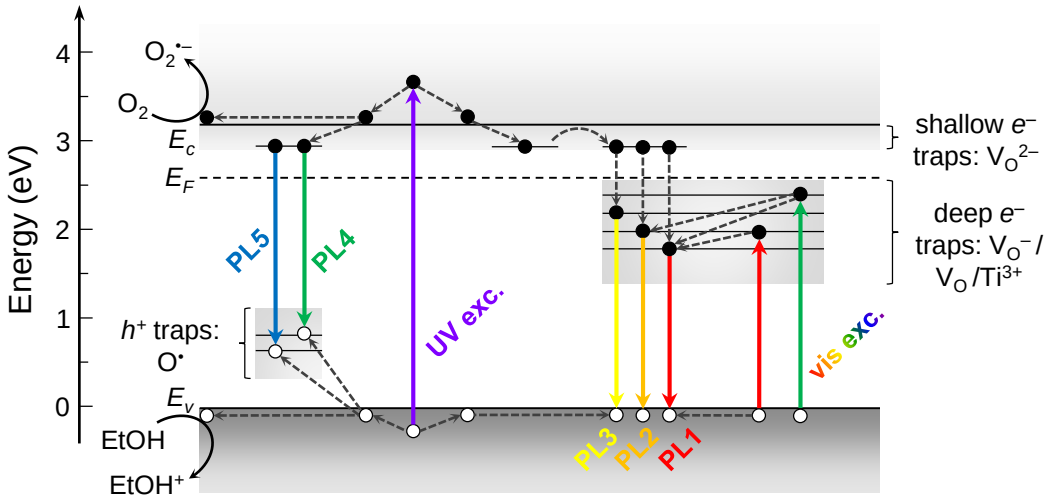

Figure 7: Schematic illustration of the possible PL mechanisms in annealed nanostructured TiO_2 films. The grey areas corresponding to shallow electron traps, deep hole traps and deep electron traps have been depicted with a width of about 0.2 eV, 0.8 eV, and 1.0 eV, respectively, based on the PL measurements (deep traps) and on the reported value of anatase Urbach energy.[61] The energy scale is reported against the valence band maximum, $E_v = 0$, so that the conduction band minimum is $E_c = 3.2$ eV, while the Fermi level is $E_F = 2.6$ eV, based on the valence band XPS measurements (Figure 1).

excitation in air.

Ethanol (Figure 6), conversely, would scavenge valence band holes, resulting in a preferential quenching of the red PL mechanism. At the same time, mobile electrons would not suffer anymore the scavenging effect by O_2 (which is absent) and could recombine with deeply-trapped holes (i.e. O$^\bullet$ radicals exposed at the surface or in the sub-surface layer). The latter could be less reactive than free holes,[62] thus "surviving" the scavenging process, as already hypothesized previously for EPR measurements in Figure 3, occurring in a H_2O/MeOH mixture. As a consequence, the green PL mechanism may be activated, producing a blueshift in the PL curves in Figure 6. Notably, the highest-energy component, i.e. $PL_{5,UV}$, having $\varepsilon_{5,UV} = 2.49$ eV, has been ascribed to the green PL mechanism and not to the self-trapped exciton recombination (reported at 2.95 eV for mesoporous anatase TiO_2[19] and 2.5 eV for anatase single crystals)[58] due to its occurrence together with the green component, i.e. $PL_{4,UV}$. The incomplete quenching of the red PL mechanism in these conditions (see also Figures S6–S9 and Table 2) may be related to the presence of non-scavenged holes due to their generation "far away" from the surface, as suggested by their low diffusion length in

TiO_2 (about 10 nm).[70] It should also be noted that PL experiments in ethanol (Figures 5a and 5c) and EPR experiments with spin-trapping agent in the presence of methanol (Figure 3) provide an indication on the charge trapping and recombination processes occurring during water splitting experiments in the presence of a hole scavenger.

Finally, by removing any surrounding medium and performing the PL measurements in vacuum, the scavenging of mobile electrons would not come into play, thus increasing the intensity of PL in Figure 6 for most of the investigated films. However, no green PL seem to occur in this case, as the spectral shape of PL curves recorded in vacuum is completely comparable to that of PL curves recorded in air. Thus, it may be hypothesized that, for these hierarchical TiO_2 films, the red PL may be a sort of "preferred" mechanism, possibly related to a lower concentration of hole traps (i.e. O-based radicals only in the first surface layers) with respect to electron traps (i.e. Ti^{3+} ions in the sub-surface layers and/or in the bulk). TiO_2 nanostructured films prepared in similar conditions to the present study (by ablating a TiO_2 target in pure O_2 atmosphere at 7 Pa) showed an evident green PL with UV excitation.[23] In this case, however, the use of a mixed Ar/O_2 atmosphere during deposition may induce the formation of Ti^{3+} states in the whole thickness of the film, which would "survive" the annealing processes[33,34] and lead to the observed red PL mechanism.

PL with visible excitations. The observation of PL with sub-bandgap excitation has already been reported in few works, i.e. with blue[20,23] and green[15,32] excitations. Pallotti *et al.*, in particular, suggested that sub-bandgap excitation (2.8 eV) can promote electrons to shallow states, which then migrate into deeper traps and, eventually, radiatively recombine with valence band holes according to the red PL mechanism.[23] Other authors reported a PL peaking at 2.15 eV (yellow) with 2.4 eV excitation (green).[15,32] Thus, the results presented in Figure 4b and 4c may be compared to those studies, since the PL curves exhibited peaks in the orange and red regions of the visible electromagnetic spectrum, consistently with the red PL mechanism. Indeed, Rex *et al.* have shown that the red PL mechanism could be characterized by more than a single emission: an additional peak in the yellow region was detected

by means of spectroelectrochemical experiments.[71] However, the measurements with blue excitation (Figure 4b) present a somehow conflicting picture, as for the TiO_2-V and TiO_2-H film the PL curve could be fitted with a single Gaussian peak in the green (see Tables 1, S5, and S6). This effect has not been fully clarified and the recombination pathway upon blue light excitation was not represented in Figure 7. Further experiments, such as photoluminescence excitation spectroscopy (PLE),[23] may be required for a clearer understanding of those results. Moreover, differently to previous studies (to the authors' knowledge), this work presents the observation of PL with red excitation (1.96 eV, see Figure 4d), which can be interpreted with the same argument as above, i.e. in terms of the red PL mechanism. In this case, the lowest-energy component would indeed be observed (i.e. the PL_1 peak at 1.8 eV).

Another interesting feature is the absence of blueshift for PL curves measured in ethanol (Figure 5c) and in vacuum (Figure 5d) with respect to air (Figure 4c). i) In these conditions only the red PL mechanism is expected, because the green PL process would be activated by above-bandgap excitation. The former is mediated by deeply-trapped electrons, which are much less sensitive to the O_2 scavenging effect.[20,23] ii) On the other hand, deeply-trapped electrons, in addition to those already present at equilibrium, can be directly photoexcited with visible irradiation (i.e. direct photoexcitation of electrons from the valence band to deep traps).[10] The resulting photoexcited holes in the valence band could be scavenged by ethanol, quenching the red PL mechanism. Since this does not occur in Figure 5c, the photogeneration process may occur relatively "far away" from the surface, due to the low absorption cross-section of TiO_2 for energies lower than the bandgap. As a consequence, by excluding both the scavenging of deeply-trapped electrons by O_2 (i) and of valence band holes by ethanol (ii), the PL measured under green excitation in all the investigated media should be similar for each TiO_2 film, as in Figure 4c (air), Figure 5c (ethanol), and Figure 5d (vacuum).

Annealing effects. In this work, both the effects of oxidizing/reducing thermal treat-

ments and different surrounding media on PL measurements have been taken into account, as rarely performed in most of the previous studies on the same topic. A previous work employing a similar methodology was reported by Rex *et al.*,[27] who performed spectroelectrochemical PL measurements on pristine and H_2-annealed rutile TiO_2 nanowires.

The main observation related to the effect of the various thermal treatments is that they give rise to clear intensity trends either with sub-bandgap excitations (Figures 4b, 4c, 5c, and 5d), or with UV excitation in ethanol (Figure 5a). In both cases, the PL intensity trend with respect to annealing is TiO_2-AH $>$ TiO_2-H $>$ TiO_2-V $>$ $TiO_2 \simeq 0$. The negligible signal for the TiO_2 film in those conditions is consistent with previous results obtained with thicker films with analogous synthesis and annealing parameters,[33] but in contrast to other studies.[15,20,23,32] Similar PL intensities for all the annealed films, instead, appeared with UV excitation in air and in vacuum (Figures 4a and 5b).

To explain such observations, it may be hypothesized that: i) the concentration of defects induced by thermal treatments in the TiO_2 thin films varies along the distance from the surface; ii) the location of photoexcited charge carriers may also vary depending on the incident wavelength. The second point can be understood by considering estimates of the light penetration depth in the TiO_2 films based on optical spectroscopy measurements.[33,34] The values of $\simeq$ 170 nm, $\simeq$ 7 µm, and $\geq$ 10 µm were obtained respectively for UV, blue, and green or red excitation energies, respectively. This suggests that the UV light is fully absorbed within the film thickness (as expected), on the contrary of visible light, which travels along the whole film being poorly absorbed. These are approximate values valid for all the films, since their optical properties were only slightly influenced by the different thermal treatments.[33,34]

Let us first consider deep electron traps. i) Lattice-embedded Ti^{3+} defects may be present in similar concentrations in the first surface layers of all the TiO_2 films but higher in the "bulk" of the reduced films, especially for the TiO_2-AH, possibly due to diffusion phenomena during thermal treatments. ii) The region for UV excitation absorption would occur in the

first tens of nm of TiO_2 nanostructured films due to the short penetration depth, while visible excitations would be (poorly) absorbed in the whole film. The observations i) and ii) together could explain the similar intensities of PL spectra for all the films with UV excitation in air and in vacuum (Figures 4a and 5b) and the different intensities observed with visible excitations (Figures 4b and 4c).

Let us now consider deep hole traps. i) The TiO_2 film may be characterized by the presence of surface-exposed O radicals, while the reduced films by additional hole traps (i.e. in the subsurface) with greater stability against the hole scavenging effect of alcohols, especially in the TiO_2-H film. ii) As previously, UV excitation would be absorbed in the first tens of nm, while visible excitation in the whole film. As a consequence, the observations i) and ii) together could explain the highest PL intensity for the TiO_2-H film in ethanol with UV excitation and, in general, higher for the reduced films with respect to the TiO_2 film (Figure 5a).

Alternative hypotheses with respect to the above discussion may also be made. For instance, the different thermal treatments could allow additional excitation pathways for the photoexcitation of electron-hole pairs, without changing the energy levels of deep electron luminescent traps. In this regard, the TiO_2 film would have few light-absorbing electron traps, thus showing no red PL with sub-bandgap excitation (Figures 4b–4d), as well as hole traps, thus exhibiting a negligible green PL in ethanol (Figure 5a). A different perspective would consist in taking into account the role of non-radiative recombinations, which are indeed significant in anatase TiO_2.[19,24] In this regard, the higher PL signal for the TiO_2-AH film with visible excitation with respect to all the other films (Figures 4b–4d) may indicate a lower degree of non-radiative recombinations for the former. This hypothesis could agree with the general observation of improved charge carrier conduction and increased photocurrents in reduced TiO_2 materials as photoanodes, as a result of lower charge recombinations.[72–74]

We point out that the PL intensity trends in this work do not correlate, nor anti-correlate, with the photoconversion efficiency trends reported in our previous investigations on TiO_2

photoanodes prepared in analogous conditions.[33,34] This can be understood considering, on the one hand, the effect of the surrounding medium (PEC experiments were performed in 0.1 M KOH solution), and that of non-radiative recombinations, as already mentioned. Spectroelectrochemical experiments, as performed by McHale and co-workers,[26,27] may be required to find a more reliable correlation between PL intensity and photocurrent density of photoelectrode materials.

The different hypotheses presented above can partially explain the results of this work, but at the moment the identification of the precise underlying mechanism is hardly possible, due to the complexity of the current observations. Similarly, the identification of deep electron traps as Ti^{3+} ions in the lattice and of deep hole traps as surface/sub-surface $O^{\bullet}$ radicals should be considered as a hypothesis and not as a unquestionable answer. Nevertheless, the results presented here suggest the important role of PL spectroscopy as a technique to detect low concentrations of defects in TiO_2 nanostructures formed by reducing thermal treatments.

4 Conclusions

We have presented a study on the PL properties of reduced anatase TiO_2 nanostructured films, in which various effects have been considered to search for a better understanding on the radiative recombination processes. While the concentration of defects is below the detection limit of XPS, EPR spectroscopy can identify the presence of Ti^{3+} ions as electron traps at the solid state and oxygen-based radicals as hole traps with the aid of a spin-trapping agent. Moreover, clear differences related to the annealing treatments appear in PL spectra. Indeed, while measurements with UV excitation in air show a similar emission for all the films, interpreted in terms of the red PL mechanism for anatase TiO_2,[19] intensity trends related to the thermal treatment appear with UV excitation in ethanol and with all the visible excitations in any surrounding medium. This is attributed, on the one hand, to a

different degree of surface hole traps introduced by thermal treatments (i.e. oxygen-based radicals), giving rise to the green PL mechanism. On the other hand, results with sub-bandgap excitation could be interpreted in terms of different concentrations of Ti^{3+} ions in the sub-surface layers of TiO_2, also in this case related to the specific annealing atmosphere. Conversely, the concentration of such states close to the surface may be more similar between all the investigated films. However, the effects of non-radiative recombinations, which could not be directly probed in this study, hinder a straightforward identification of the underlying processes.

The present findings elucidate once more the complexity of PL processes in TiO_2 materials, which require further investigations to achieve a more general understanding. The same holds for a unequivocal physical-chemical identification of the nature of electron and hole traps. A thorough knowledge on the radiative as well as non-radiative recombination processes in the material could allow a fine tuning of the photoactivity and efficiency of TiO_2-based solar energy conversion devices. Steady-state PL spectroscopy could be coupled with other techniques, such as EPR, time-resolved PL, and transient absorption (TA) spectroscopy.[24] Moreover, DFT simulations of realistic systems should be also considered to pursue such a challenging task.[53] A similar methodology could be applied to gain further understanding on other Earth-abundant oxides typically employed for photocatalysis/water splitting applications (i.e. Fe_2O_3, $BiVO_4$), yielding to higher solar energy conversion performances.

Acknowledgement

A.N. and Š.K. gratefully acknowledge the support by the Operational Programme Research, Development and Education - European Regional Development Fund, project no. CZ.02.1.01/0.0/0.0/15_003/0000416 of the Ministry of Education, Youth and Sports of the Czech Republic. We thank Claudia Aparicio for her aid in XRD measurements and Martin

Petr for his aid in XPS measurements.

Supporting Information Available

The Supporting Information is available free of charge ...

Additional experimental details on the characterization of TiO_2 films; SEM, Raman and XRD measurements; O 1s, Ti 2p, and C 1s XPS spectra; additional details on DFT simulations; multi-Gaussian fitting of PL curves.

References

(1) Hagfeldt, A.; Boschloo, G.; Sun, L.; Kloo, L.; Pettersson, H. Dye-Sensitized Solar Cells. *Chem. Rev.* **2010**, *110*, 6595–6663.

(2) Kavan, L. Electrochemistry and dye-sensitized solar cells. *Curr. Opin. Electrochem.* **2017**, *2*, 88–96.

(3) Kavan, L. Electrochemistry and perovskite photovoltaics. *Curr. Opin. Electrochem.* **2018**, *11*, 122–129.

(4) Kavan, L. Conduction band engineering in semiconducting oxides (TiO_2, SnO_2): Applications in perovskite photovoltaics and beyond. *Catal. Today* **2019**, *328*, 50–56.

(5) Fujishima, A.; Zhang, X.; Tryk, D. A. TiO_2 photocatalysis and related surface phenomena. *Surf. Sci. Rep.* **2008**, *63*, 515–582.

(6) Schneider, J.; Matsuoka, M.; Takeuchi, M.; Zhang, J.; Horiuchi, Y.; Anpo, M.; Bahnemann, D. W. Understanding TiO_2 Photocatalysis: Mechanisms and Materials. *Chem. Rev.* **2014**, *114*, 9919–9986.

(7) Kment, S.; Riboni, F.; Pausova, S.; Wang, L.; Wang, L.; Han, H.; Hubicka, Z.; Krysa, J.; Schmuki, P.; Zboril, R. Photoanodes based on TiO_2 and α-Fe_2O_3 for solar water splitting – superior role of 1D nanoarchitectures and of combined heterostructures. *Chem. Soc. Rev.* **2017**, *46*, 3716–3769.

(8) Nowotny, J.; Bak, T.; Nowotny, M. K.; Sheppard, L. R. Titanium dioxide for solar-hydrogen II. Defect chemistry. *Int. J. Hydrogen Energ.* **2007**, *32*, 2630–2643.

(9) Cronemeyer, D. C. Electrical and Optical Properties of Rutile Single Crystals. *Phys. Rev.* **1952**, *87*, 876–886, 00537.

(10) Chen, X.; Liu, L.; Huang, F. Black titanium dioxide (TiO_2) nanomaterials. *Chem. Soc. Rev.* **2015**, *44*, 1861–1885.

(11) Naldoni, A.; Altomare, M.; Zoppellaro, G.; Liu, N.; Kment, S.; Zbořil, R.; Schmuki, P. Photocatalysis with Reduced TiO_2: From Black TiO_2 to Cocatalyst-Free Hydrogen Production. *ACS Catal.* **2019**, *9*, 345–364.

(12) Chen, X.; Liu, L.; Yu, P. Y.; Mao, S. S. Increasing Solar Absorption for Photocatalysis with Black Hydrogenated Titanium Dioxide Nanocrystals. *Science* **2011**, *331*, 746–750.

(13) Gfroerer, T. H. In *Photoluminescence in Analysis of Surfaces and Interfaces*; Meyers, R. A., Ed.; John Wiley & Sons, Ltd, 2006; pp 9209–9231.

(14) McHale, J. L.; Knorr, F. J. In *Handbook of Luminescent Semiconductor Materials*; Bergman, L., McHale, J. L., Eds.; CRC Press, 2012; pp 365–390.

(15) Zhang, W. F.; Zhang, M. S.; Yin, Z.; Chen, Q. Photoluminescence in anatase titanium dioxide nanocrystals. *Appl. Phys. B* **2000**, *70*, 261–265.

(16) Bieber, H.; Gilliot, P.; Gallart, M.; Keller, N.; Keller, V.; Bégin-Colin, S.; Pighini, C.; Millot, N. Temperature dependent photoluminescence of photocatalytically active titania nanopowders. *Catal. Today* **2007**, *122*, 101–108.

(17) Shi, J.; Chen, J.; Feng, Z.; Chen, T.; Lian, Y.; Wang, X.; Li, C. Photoluminescence Characteristics of TiO_2 and Their Relationship to the Photoassisted Reaction of Water/Methanol Mixture. *J. Phys. Chem. C* **2007**, *111*, 693–699.

(18) Iijima, K.; Goto, M.; Enomoto, S.; Kunugita, H.; Ema, K.; Tsukamoto, M.; Ichikawa, N.; Sakama, H. Influence of oxygen vacancies on optical properties of anatase TiO_2 thin films. *J. Lumin.* **2008**, *128*, 911–913.

(19) Knorr, F. J.; Mercado, C. C.; McHale, J. L. Trap-State Distributions and Carrier Transport in Pure and Mixed-Phase TiO_2 Influence of Contacting Solvent and Interphasial Electron Transfer. *J. Phys. Chem. C* **2008**, *112*, 12786–12794.

(20) Preclíková, J.; Galář, P.; Trojánek, F.; Daniš, S.; Rezek, B.; Gregora, I.; Němcová, Y.; Malý, P. Nanocrystalline titanium dioxide films: Influence of ambient conditions on surface- and volume-related photoluminescence. *J. Appl. Phys.* **2010**, *108*, 113502.

(21) Wang, X.; Feng, Z.; Shi, J.; Jia, G.; Shen, S.; Zhou, J.; Li, C. Trap states and carrier dynamics of TiO_2 studied by photoluminescence spectroscopy under weak excitation condition. *Phys. Chem. Chem. Phys.* **2010**, *12*, 7083–7090.

(22) Stevanovic, A.; Büttner, M.; Zhang, Z.; Yates, J. T. Photoluminescence of TiO_2: Effect of UV Light and Adsorbed Molecules on Surface Band Structure. *J. Am. Chem. Soc.* **2012**, *134*, 324–332.

(23) Pallotti, D. K.; Passoni, L.; Maddalena, P.; Di Fonzo, F.; Lettieri, S. Photoluminescence Mechanisms in Anatase and Rutile TiO_2. *J. Phys. Chem. C* **2017**, *121*, 9011–9021.

(24) Vequizo, J. J. M.; Kamimura, S.; Ohno, T.; Yamakata, A. Oxygen induced enhancement of NIR emission in brookite TiO_2 powders: comparison with rutile and anatase TiO_2 powders. *Phys. Chem. Chem. Phys.* **2018**, *20*, 3241–3248.

(25) Mercado, C. C.; Knorr, F. J.; McHale, J. L.; Usmani, S. M.; Ichimura, A. S.; Saraf, L. V. Location of Hole and Electron Traps on Nanocrystalline Anatase TiO_2. *J. Phys. Chem. C* **2012**, *116*, 10796–10804.

(26) Knorr, F. J.; McHale, J. L. Spectroelectrochemical Photoluminescence of Trap States of Nanocrystalline TiO_2 in Aqueous Media. *J. Phys. Chem. C* **2013**, *117*, 13654–13662.

(27) Rex, R. E.; Yang, Y.; Knorr, F. J.; Zhang, J. Z.; Li, Y.; McHale, J. L. Spectroelectrochemical Photoluminescence of Trap States in H-Treated Rutile TiO_2 Nanowires: Implications for Photooxidation of Water. *J. Phys. Chem. C* **2016**, *120*, 3530–3541.

(28) Yan, Y.; Han, M.; Konkin, A.; Koppe, T.; Wang, D.; Andreu, T.; Chen, G.; Vetter, U.; Morante, J. R.; Schaaf, P. Slightly hydrogenated TiO_2 with enhanced photocatalytic performance. *J. Mater. Chem. A* **2014**, *2*, 12708–12716.

(29) Liu, N.; Schneider, C.; Freitag, D.; Venkatesan, U.; Marthala, V. R. R.; Hartmann, M.; Winter, B.; Spiecker, E.; Osvet, A.; Zolnhofer, E. M.; Meyer, K.; Nakajima, T.; Zhou, X.; Schmuki, P. Hydrogenated Anatase: Strong Photocatalytic Dihydrogen Evolution without the Use of a Co-Catalyst. *Angew. Chem.* **2014**, *126*, 14425–14429.

(30) Gurylev, V.; Su, C.-Y.; Perng, T.-P. Surface reconstruction, oxygen vacancy distribution and photocatalytic activity of hydrogenated titanium oxide thin film. *J. Catal.* **2015**, *330*, 177–186.

(31) Rex, R. E.; Knorr, F. J.; McHale, J. L. Comment on "Characterization of Oxygen Vacancy Associates within Hydrogenated TiO_2: A Positron Annihilation Study". *J. Phys. Chem. C* **2013**, *117*, 7949–7951.

(32) Šćepanović, M.; Dohčević-Mitrović, Z.; Hinić, I.; Grujić-Brojčin, M.; Stanišić, G.; Popović, Z. V. Photoluminescence of Laser-Synthesized Anatase Titanium Dioxide Nanopowders. *Mater. Sci. Forum* **2005**, *494*, 265–270.

(33) Mascaretti, L.; Ferrulli, S.; Mazzolini, P.; Casari, C. S.; Russo, V.; Matarrese, R.; Nova, I.; Terraneo, G.; Liu, N.; Schmuki, P.; Li Bassi, A. Hydrogen-treated hierarchical titanium oxide nanostructures for photoelectrochemical water splitting. *Sol. Energy Mater. Sol. Cells* **2017**, *169*, 19–27.

(34) Mascaretti, L.; Matarrese, R.; Ravanelli, A.; Isacchi, M.; Mazzolini, P.; Casari, C. S.; Russo, V.; Nova, I.; Terraneo, G.; Ducati, C.; Li Bassi, A. Tuning the photoelectrochemical properties of hierarchical TiO_2 nanostructures by control of pulsed laser deposition and annealing in reducing conditions. *Int. J. Hydrogen Energ.* **2017**, *42*, 26639–26651.

(35) Tajima, M.; Ogura, A.; Karasawa, T.; Mizoguchi, A. Defect Analysis in Bonded and H^+ Split Silicon-on-Insulator Wafers by Photoluminescence Spectroscopy and Transmission Electron Microscopy. *Jpn. J. Appl. Phys.* **1998**, *37*, L1199.

(36) Sauvage, F.; Di Fonzo, F.; Li Bassi, A.; Casari, C. S.; Russo, V.; Divitini, G.; Ducati, C.; Bottani, C. E.; Comte, P.; Grätzel, M. Hierarchical TiO_2 Photoanode for Dye-Sensitized Solar Cells. *Nano Lett.* **2010**, *10*, 2562–2567.

(37) Passoni, L.; Ghods, F.; Docampo, P.; Abrusci, A.; Martí-Rujas, J.; Ghidelli, M.; Divitini, G.; Ducati, C.; Binda, M.; Guarnera, S.; Li Bassi, A.; Casari, C. S.; Snaith, H. J.; Petrozza, A.; Di Fonzo, F. Hyperbranched Quasi-1D Nanostructures for Solid-State Dye-Sensitized Solar Cells. *ACS Nano* **2013**, *7*, 10023–10031.

(38) Matarrese, R.; Nova, I.; Li Bassi, A.; Casari, C. S.; Russo, V.; Palmas, S. Preparation and optimization of TiO_2 photoanodes fabricated by pulsed laser deposition for photoelectrochemical water splitting. *J. Solid State Electrochem.* **2017**, 1–16.

(39) Wang, Z.; Yang, C.; Lin, T.; Yin, H.; Chen, P.; Wan, D.; Xu, F.; Huang, F.; Lin, J.; Xie, X.; Jiang, M. H-Doped Black Titania with Very High Solar Absorption and Excellent Photocatalysis Enhanced by Localized Surface Plasmon Resonance. *Adv. Funct. Mater.* **2013**, *23*, 5444–5450.

(40) Chen, B.; Beach, J. A.; Maurya, D.; Moore, R. B.; Priya, S. Fabrication of black hierarchical TiO_2 nanostructures with enhanced photocatalytic activity. *RSC Adv.* **2014**, *4*, 29443–29449.

(41) Wang, G.; Wang, H.; Ling, Y.; Tang, Y.; Yang, X.; Fitzmorris, R. C.; Wang, C.; Zhang, J. Z.; Li, Y. Hydrogen-Treated TiO_2 Nanowire Arrays for Photoelectrochemical Water Splitting. *Nano Lett.* **2011**, *11*, 3026–3033.

(42) Naldoni, A.; Allieta, M.; Santangelo, S.; Marelli, M.; Fabbri, F.; Cappelli, S.; Bianchi, C. L.; Psaro, R.; Dal Santo, V. Effect of Nature and Location of Defects on Bandgap Narrowing in Black TiO_2 Nanoparticles. *J. Am. Chem. Soc.* **2012**, *134*, 7600–7603.

(43) Sanjinés, R.; Tang, H.; Berger, H.; Gozzo, F.; Margaritondo, G.; Lévy, F. Electronic structure of anatase TiO_2 oxide. *J. Appl. Phys.* **1994**, *75*, 2945–2951.

(44) Prince, K. C.; Dhanak, V. R.; Finetti, P.; Walsh, J. F.; Davis, R.; Muryn, C. A.; Dhariwal, H. S.; Thornton, G.; Van der Laan, G. 2p resonant photoemission study of TiO_2. *Phys. Rev. B* **1997**, *55*, 9520–9523, 00041.

(45) Fusi, M.; Maccallini, E.; Caruso, T.; Casari, C. S.; Li Bassi, A.; Bottani, C. E.; Rudolf, P.; Prince, K. C.; Agostino, R. G. Surface electronic and structural properties of nanostructured titanium oxide grown by pulsed laser deposition. *Surf. Sci.* **2011**, *605*, 333–340.

(46) Wendt, S.; Sprunger, P. T.; Lira, E.; Madsen, G. K. H.; Li, Z.; Hansen, J. Ø.; Matthiesen, J.; Blekinge-Rasmussen, A.; Lægsgaard, E.; Hammer, B.; Besenbacher, F. The Role of Interstitial Sites in the Ti3d Defect State in the Band Gap of Titania. *Science* **2008**, *320*, 1755–1759.

(47) Livraghi, S.; Chiesa, M.; Paganini, M. C.; Giamello, E. On the Nature of Reduced

States in Titanium Dioxide As Monitored by Electron Paramagnetic Resonance. I: The Anatase Case. *J. Phys. Chem. C* **2011**, *115*, 25413–25421.

(48) Chiesa, M.; Paganini, M. C.; Livraghi, S.; Giamello, E. Charge trapping in TiO_2 polymorphs as seen by Electron Paramagnetic Resonance spectroscopy. *Phys. Chem. Chem. Phys.* **2013**, *15*, 9435–9447.

(49) The correspondance between the notation adopted in Equations (1) and (3) to (5) and the Kröger-Vink notation is the following: $Ti^{4+}=Ti_{Ti}^{\times}$, $O^{2-}=O_O^{\times}$, $Ti^{3+}=e'$, $V_O^{2-}=V_O^{\times}$, $V_O^{-}=V_O^{\bullet}$, and $V_O=V_O^{\bullet\bullet}$.

(50) Chen, T.; Feng, Z.; Wu, G.; Shi, J.; Ma, G.; Ying, P.; Li, C. Mechanistic Studies of Photocatalytic Reaction of Methanol for Hydrogen Production on Pt/TiO_2 by in situ Fourier Transform IR and Time-Resolved IR Spectroscopy. *J. Phys. Chem. C* **2007**, *111*, 8005–8014.

(51) Uddin, M. T.; Babot, O.; Thomas, L.; Olivier, C.; Redaelli, M.; D'Arienzo, M.; Morazzoni, F.; Jaegermann, W.; Rockstroh, N.; Junge, H. New insights into the photocatalytic properties of RuO_2/TiO_2 mesoporous heterostructures for hydrogen production and organic pollutant photodecomposition. *J. Phys. Chem. C* **2015**, *119*, 7006–7015.

(52) Panarelli, E. G.; Livraghi, S.; Maurelli, S.; Polliotto, V.; Chiesa, M.; Giamello, E. Role of surface water molecules in stabilizing trapped hole centres in titanium dioxide (anatase) as monitored by electron paramagnetic resonance. *J. Photochem. Photobiol. A* **2016**, *322-323*, 27–34.

(53) Shirai, K.; Fazio, G.; Sugimoto, T.; Selli, D.; Ferraro, L.; Watanabe, K.; Haruta, M.; Ohtani, B.; Kurata, H.; Di Valentin, C.; Matsumoto, Y. Water-Assisted Hole Trapping at the Highly Curved Surface of Nano-TiO_2 Photocatalyst. *J. Am. Chem. Soc.* **2018**, *140*, 1415–1422, 00010.

(54) Tamaki, Y.; Furube, A.; Murai, M.; Hara, K.; Katoh, R.; Tachiya, M. Direct Observation of Reactive Trapped Holes in TiO_2 Undergoing Photocatalytic Oxidation of Adsorbed Alcohols: Evaluation of the Reaction Rates and Yields. *J. Am. Chem. Soc.* **2006**, *128*, 416–417.

(55) Larsen, J. K.; Li, S.-Y.; Scragg, J. J. S.; Ren, Y.; Hägglund, C.; Heinemann, M. D.; Kretzschmar, S.; Unold, T.; Platzer-Björkman, C. Interference effects in photoluminescence spectra of Cu_2ZnSnS_4 and $Cu(In,Ga)Se_2$ thin films. *J. Appl. Phys.* **2015**, *118*, 035307.

(56) Wolter, M. H.; Bissig, B.; Reinhard, P.; Buecheler, S.; Jackson, P.; Siebentritt, S. Correcting for interference effects in the photoluminescence of $Cu(In,Ga)Se_2$ thin films. *Phys. Status Solidi C* **2017**, *14*, 1600189.

(57) Peiró, A. M.; Colombo, C.; Doyle, G.; Nelson, J.; Mills, A.; Durrant, J. R. Photochemical Reduction of Oxygen Adsorbed to Nanocrystalline TiO_2 Films: A Transient Absorption and Oxygen Scavenging Study of Different TiO_2 Preparations. *J. Phys. Chem. B* **2006**, *110*, 23255–23263.

(58) Tang, H.; Berger, H.; Schmid, P. E.; Lévy, F.; Burri, G. Photoluminescence in TiO_2 anatase single crystals. *Solid. State Commun.* **1993**, *87*, 847–850, 00583.

(59) Albery, W. J.; Bartlett, P. N. The Transport and Kinetics of Photogenerated Carriers in Colloidal Semiconductor Electrode Particles. *J. Electrochem. Soc.* **1984**, *131*, 315–325.

(60) Wang, Q.; Zhang, Z.; Zakeeruddin, S. M.; Grätzel, M. Enhancement of the Performance of Dye-Sensitized Solar Cell by Formation of Shallow Transport Levels under Visible Light Illumination. *J. Phys. Chem. C* **2008**, *112*, 7084–7092.

(61) Tang, H.; Lévy, F.; Berger, H.; Schmid, P. E. Urbach tail of anatase TiO_2. *Phys. Rev. B* **1995**, *52*, 7771–7774.

(62) Bahnemann, D. W.; Hilgendorff, M.; Memming, R. Charge Carrier Dynamics at TiO_2 Particles: Reactivity of Free and Trapped Holes. *J. Phys. Chem. B* **1997**, *101*, 4265–4275, 00393.

(63) Tamaki, Y.; Furube, A.; Murai, M.; Hara, K.; Katoh, R.; Tachiya, M. Dynamics of efficient electron–hole separation in TiO_2 nanoparticles revealed by femtosecond transient absorption spectroscopy under the weak-excitation condition. *Phys. Chem. Chem. Phys.* **2007**, *9*, 1453–1460.

(64) Mazzolini, P.; Gondoni, P.; Russo, V.; Chrastina, D.; Casari, C. S.; Li Bassi, A. Tuning of Electrical and Optical Properties of Highly Conducting and Transparent Ta-Doped TiO_2 Polycrystalline Films. *J. Phys. Chem. C* **2015**, *119*, 6988–6997.

(65) Mattioli, G.; Alippi, P.; Filippone, F.; Caminiti, R.; Amore Bonapasta, A. Deep versus Shallow Behavior of Intrinsic Defects in Rutile and Anatase TiO_2 Polymorphs. *J. Phys. Chem. C* **2010**, *114*, 21694–21704.

(66) Deák, P.; Aradi, B.; Frauenheim, T. Quantitative theory of the oxygen vacancy and carrier self-trapping in bulk TiO_2. *Phys. Rev. B* **2012**, *86*, 195206.

(67) Gerosa, M.; Bottani, C. E.; Caramella, L.; Onida, G.; Di Valentin, C.; Pacchioni, G. Defect calculations in semiconductors through a dielectric-dependent hybrid DFT functional: The case of oxygen vacancies in metal oxides. *J. Chem. Phys.* **2015**, *143*, 134702.

(68) Di Valentin, C.; Pacchioni, G.; Selloni, A. Reduced and n-Type Doped TiO_2: Nature of Ti^{3+} Species. *J. Phys. Chem. C* **2009**, *113*, 20543–20552.

(69) Diebold, U. The surface science of titanium dioxide. *Surf. Sci. Rep.* **2003**, *48*, 53–229.

(70) Salvador, P. Hole diffusion length in n-TiO_2 single crystals and sintered electrodes: Photoelectrochemical determination and comparative analysis. *J. Appl. Phys.* **1984**, *55*, 2977–2985.

(71) Rex, R. E.; Knorr, F. J.; McHale, J. L. Surface Traps of TiO_2 Nanosheets and Nanoparticles as Illuminated by Spectroelectrochemical Photoluminescence. *J. Phys. Chem. C* **2014**, *118*, 16831–16841.

(72) Liu, N.; Schneider, C.; Freitag, D.; Hartmann, M.; Venkatesan, U.; Müller, J.; Spiecker, E.; Schmuki, P. Black TiO_2 Nanotubes: Cocatalyst-Free Open-Circuit Hydrogen Generation. *Nano Lett.* **2014**, *14*, 3309–3313.

(73) Liu, N.; Schneider, C.; Freitag, D.; Zolnhofer, E. M.; Meyer, K.; Schmuki, P. Noble-Metal-Free Photocatalytic H_2 Generation: Active and Inactive 'Black' TiO_2 Nanotubes and Synergistic Effects. *Chem. Eur. J.* **2016**, *22*, 13810–13814.

(74) Lu, Z.; Yip, C.-T.; Wang, L.; Huang, H.; Zhou, L. Hydrogenated TiO_2 Nanotube Arrays as High-Rate Anodes for Lithium-Ion Microbatteries. *ChemPlusChem* **2012**, *77*, 991–1000, 00111.

Graphical TOC Entry